Received: 12 November 2018 | Revised: 22 January 2019 | Accepted: 24 January 2019

DOI: 10.1002/jcp.28317

ORIGINAL RESEARCH ARTICLE

WILEY Journal of Cellular Physiology

Thioredoxin-interacting protein deficiency alleviates phenotypic alterations of podocytes via inhibition of mTOR activation in diabetic nephropathy

Shan Song[1] | Duojun Qiu[1] | Yonghong Shi[1,2] | Shuai Wang[1] | Xinbo Zhou[1] | Nan Chen[1] | Jinying Wei[1,2] | Ming Wu[1] | Haijiang Wu[1,2] | Huijun Duan[1,2]

[1]Department of Pathology, Hebei Medical University, Shijiazhuang, China

[2]Hebei Key Laboratory of Kidney Diseases, Shijiazhuang, China

Correspondence
Yonghong Shi, and Huijun Duan, Department of Pathology, Hebei Medical University, No. 361 East Zhongshan Road, Shijiazhuang, 050017 Hebei, China.
Email: yonghongshi@126.com (Y.S.); duanhj999@163.com (H.D.)

Funding information
National Natural Science Foundation of China, Grant/Award Numbers: 81270804, 81470966; China Postdoctoral Science Foundation, Grant/Award Number: 2014M561199; Hebei Human Resources and Social Security Department Project, Grant/Award Number: A2017003080

Abstract

Thioredoxin-interacting protein (TXNIP) is induced by high glucose (HG), whereupon it acts to inhibit thioredoxin, thereby promoting oxidative stress. We have found that TXNIP knockdown in human renal tubular cells helped prevent the epithelial-to-mesenchymal transition (EMT). Here, we studied the potential effect of TXNIP on podocyte phenotypic alterations in diabetic nephropathy (DN) in vivo and in vitro. In conditionally immortalized mouse podocytes under HG conditions, knocking down TXNIP disrupted EMT, reactive oxygen species (ROS) production, and mammalian target of rapamycin (mTOR) pathway activation. Further, Raptor short hairpin RNA (shRNA), Rictor shRNA, and mTOR specific inhibitor KU-0063794 were used to assess if the mTOR signal pathway is involved in HG-induced EMT in podocytes. We found that Raptor shRNA, Rictor shRNA, and KU-0063794 could all restrain HG-induced EMT and ROS production in podocytes. In addition, antioxidant Tempol or *N*-acetylcysteine presented a prohibitive effect on HG-induced EMT in podocytes. Streptozotocin was utilized to render equally diabetic in wild-type (WT) control and TXNIP$^{-/-}$ (TKO) mice. Diabetes did not increase levels of 24-hr urinary protein, serum creatinine, blood urea nitrogen, and triglyceride in TXNIP$^{-/-}$ mice. Podocyte phenotypic alterations and podocyte loss were detected in WT but not in TKO diabetic mice. Oxidative stress was also suppressed in diabetic TKO mice relative to WT controls. Also, TXNIP deficiency suppresses the activation of mTOR in glomeruli of streptozotocin-induced diabetic mice. Moreover, TXNIP expression, mTOR activation, Nox1, and Nox4 could be detected in renal biopsy tissues of patients with DN. This suggests that decreased TXNIP could ameliorate phenotypic alterations of podocytes via inhibition of mTOR in DN, highlighting TXNIP as a promising therapeutic target.

KEYWORDS
diabetic nephropathy, EMT, mTOR, ROS, TXNIP

1 | INTRODUCTION

Diabetic nephropathy (DN) manifests as a diabetic complication, which affects the microvascular system (Rask-Madsen & King, 2013), in which hyperglycemia contributes to podocyte loss and phenotypic alterations of the glomerular filtration barrier, eventually resulting in the damage of renal filtration (Dronavalli, Duka, & Bakris, 2008; Rask-Madsen & King, 2013). However, the detailed molecular pathogenesis of DN remains obscure. Specialized and terminally differentiated, podocytes are glomerular basement membrane (GBM)

epithelial cells located outside of glomerular capillaries (Benzing, 2004; Pavenstadt, Kriz, & Kretzler, 2003). During development, podocytes arise through the mesenchymal-to-epithelial transition (MET) from mesenchymal tissue, but may undergo reverse embryogenesis, epithelial-to-mesenchymal transition (EMT), which occurs in kidneys under pathological circumstances (Little & McMahon, 2012). It is universally acknowledged that renal tubular epithelial cells may well suffer EMT after chronic injury (Iwano et al., 2002; Strutz & Zeisberg, 2006; Yang & Liu, 2001). We assumed that similar to tubular EMT, phenotypic alterations of podocytes might play a crucial part in causing podocyte dysfunction, which might finally result in deficient glomerular filtration.

Among pathogenic factors, excessive reactive oxygen species (ROS) production is a key driver of DN (Giacco & Brownlee, 2010; Nishikawa et al., 2000; Rask-Madsen & King, 2013). The excess ROS may bring about the DNA and protein oxidation, interfering with form and function (Shah et al., 2015). One protein correlated with the regulation of ROS is thioredoxin-interacting protein (TXNIP), which can be remarkably enhanced under high glucose (HG) circumstances in many cells (Cheng et al., 2006; Masson et al., 2009; Perrone, Devi, Hosoya, Terasaki, & Singh, 2009; Qi et al., 2007). Through bonding with the redox-active cysteine residues to inactivate its antioxidative function, TXNIP is a Trx inhibitor (Nishiyama et al., 1999). As TXNIP is a Trx binding partner and endogenous inhibitor, it is thought to be tightly linked with cellular redox regulation (Nishiyama et al., 1999). Our previous research has proved that TXNIP knockdown could ameliorate HG or TGF-β1-induced EMT in human renal tubular cells (Wei et al., 2013), and that lack of TXNIP may alleviate renal fibrosis in mice (M. Wu et al., 2018). In addition, Shah et al (2015) illustrated that TXNIP deficiency protected diabetic mice from renal fibrosis, extracellular matrix accumulation, podocyte loss, and podocyte foot process effacement. Based on literature above, we hypothesize that TXNIP deficiency might alleviate phenotypic alterations of podocytes in DN.

Increasing evidence has indicated that DN pathogenesis is tied to the mammalian target of rapamycin (mTOR) signaling pathway. Serving as an evolutionarily conserved eukaryotic nutrient-responsive modulator of cell survival, growth, and metabolism (Godel et al., 2011; Wullschleger, Loewith, & Hall, 2006), mTOR is a serine/threonine protein kinase composed of the mTORC1 and mTORC2 functional complexes (Dann, Selvaraj, & Thomas, 2007; Sabatini, 2006). mTORC1 mediates its effects via specific kinases and through 4E-binding protein 1 (4E-BP1; Um, D'Alessio, & Thomas, 2006). The rapamycin-insensitive mTORC2 mediates Ser^{473} phosphorylation of protein kinase B (PKB/Akt; Sarbassov, Guertin, Ali, & Sabatini, 2005). Another study illustrated that mTORC1 activation makes podocytes convert into a fibroblastic phenotype and results in podocyte detachment (Inoki et al., 2011).

Herein, we investigated whether TXNIP silencing could ameliorate EMT induced by HG in podocytes by suppressing mTOR pathway. We used mouse podocytes, TXNIP knockout (TKO) mice with streptozotocin (STZ)-induced diabetes and renal biopsy tissues of patients with DN to explore the roles of TXNIP on renal injury, podocyte loss, phenotypic alterations of podocytes, oxidative stress, and its potential mechanism in DN.

2 | MATERIALS AND METHODS

2.1 | Reagents

D-glucose, *N*-acetylcysteine (NAC), mannitol, as well as STZ came from Sigma (St. Louis, MO). RPMI 1640 culture media and fetal bovine serum (FBS) came from Gibco (Gaithersburg, MD). Penicillin, streptomycin, and TRIzol were bought from Invitrogen (Carlsbad, CA). Tempol and KU-0063794 were bought from Selleck Chemicals (Houston, TX). Recombinant mouse γ-interferon was purchased from PeproTech (NJ). TXNIP short hairpin RNA (shRNA) plasmid was provided by Santa Cruz Biotechnology (CA), while Raptor shRNA plasmid, Rictor shRNA plasmid, and control plasmids were provided by GenePharma (Shanghai, China). FuGENE HD transfection reagent came from Promega Corporation (Madison, WI), while Takara (Shiga, Japan) was the source of SYBR Premix Ex Taq II. Antibodies against α-smooth muscle actin (α-SMA), E-cadherin, synaptopodin, Raptor, Rictor, p-S6, p-AKT^{SER473}, Nox1, Nox4, and β-actin came from Proteintech (Chicago, IL), while antibodies for nephrin, desmin, and Wilm's Tumor Antigen-1 (WT-1) came from Abcam (Cambridge, UK). Biochemical detection kits for 24-hr urinary protein (Upro), blood urea nitrogen (BUN), serum creatinine (Scr) along with triglyceride (TG) came from Nanjing Jiancheng Bioengineering Institute (Nanjing, China). Besides, 8-hydroxydeoxyguanosine (8-OHdG) ELISA Kit was from Elabscience Biotechnology (Wuhan, China).

2.2 | Cell culture and transfection

The Cell Culture Centre (PUMC, CAMS, Beijing, China) provided us with conditionally immortalized murine podocytes, which we grew based on previous descriptions of experimental protocols (Mundel et al., 1997). These podocytes express a temperature-sensitive SV40 large T-cell antigen under a γ-interferon regulated $H\text{-}2K^b$ promoter. For the sake of podocyte proliferation, cells were grown using RPMI 1640 culture medium at 33°C. In permissive growth conditions, the media contained 10% FBS, along with penicillin/streptomycin and 10 U/ml murine γ-interferon. Under restrictive growth conditions, the cells were grown at 37°C with media containing 10% FBS and penicillin/streptomycin, driving cells toward a quiescent differentiated state. When podocytes appeared to be 70–80% confluent, the cells would be transitioned to 37°C to differentiate for 14–20 days before use in downstream studies. Then, stable transfections of podocytes with TXNIP shRNA plasmid, Raptor shRNA plasmid, Rictor shRNA plasmid, or control plasmids was conducted via FuGENE HD transfection reagent in accordance with the provided directions. The podocytes were then grown in RPMI 1640 medium free of serum for 6 hr, and the substrate was changed into the original medium. Afterwards for stimulation, podocytes were treated using NG (5.6 mM), NG+mannitol (24.4 mM), HG (30 mM), HG + KU-0063794 (1 μM), HG + Tempol (1 mM), or HG + NAC (5 mM) for 48 hr.

TABLE 1 The sequences of the polymerase chain reaction primer pairs used in this study

Genes	Forward primers (5′→3′)	Reverse primers (5′→3′)
α-SMA	CGCCCTCGCCACCAGATCTG	TAGCCTTCATAGATGGGGAC
E-cadherin	GCCGGAGCCCTGCCACCCTG	CTTTCTGTAGGTGGAGTCCC
Nephrin	GTTCCAAGCCAAAGGATGCC	GCATGTAATGCCAGGGCT
Desmin	CCATTGCCCTGGGATGAACT	TACCCGATGCCCAGGTGATA
Synaptopodin	GCCCTCCTTCTGCTTCAAGT	TCTTCCTCACTAAGCCCCGA
Raptor	GGACTGACAGGACACGGAAC	TTCTCATCTGGCAAGGGCAG
Rictor	ACTGACGCCAAGCAGGTTTA	GGAGCGCTGGAGGGTATTG
Nox1	TTTCTCTCCCGAAGGACCTCT	TTCAGCCCCAACCAGGAAAC
Nox4	CGAGCCAAAGGGGCCCTGAAG	AACAGCGTGCGTCTAACGGCA
18s	ACACGGACAGGATTGACAGA	GGACATCTAAGGGCATCACAG

Note. α-SMA: α-smooth muscle actin

2.3 | Animals and metabolic studies

$TXNIP^{-/-}$ (TXNIP KO, TKO) C57BL/6J-derived mice (8-weeks old) were produced using the transcription activator-like effector nucleases approach (Zhang et al., 2015). Wild-type (WT) littermates served as controls. Mice received unrestricted food and water access and housing in a standard setting in the Hebei Medical University animal facility. All studies were permitted by the Animal Ethics committee of Hebei Medical University. An intraperitoneal injection of STZ (50 mg/kg, pH 4.5, prepared using 0.1 M citrate buffer) was administered to mice daily for 5 consecutive days to induce diabetes in eight mice per group, while control mice were given citrate buffer. We monitored blood glucose in mice using a glucometer (Roche, Basel, Switzerland) weekly. Sixteen weeks after STZ injection, we put individual mice in metabolic chambers individually for 24 hr to examine the urine excretion volume. We centrifuged the urine for 1 min at 1000 rpm, and it was then frozen at −80°C for follow-up analyses: Upro and 8-OHdG. After that, mice were killed and their blood was gathered for assessment of blood glucose, Scr, BUN, and TG. Meanwhile, renal tissues were collected for follow-up experiments described below. The instrument used to assess Upro, Scr, BUN, and TG was Biochrom Ultrospec 2100 pro (Biochrom Ltd., Cambridge, UK). The urinary assay for 8-OHdG was determined by a microplate reader and Gen5 software (Biotek, VT) following the manufacturer's guidelines.

2.4 | Human renal biopsies

Human renal biopsy tissues were collected in the Second Hospital of Hebei Medical University. This study was approved by Hebei Medical University ethical committees. Informed consents were obtained from patients according to approved guidelines. There were altogether 16 kidney biopsies from individual patients in our study: 12 samples were from individuals suffering from type 2 diabetes with DN confirmed by biopsy and four samples from normal control patients. The normal control renal tissues were achieved from the intact normal pole of nephrectomy samples of individuals who suffered circumscribed solitary renal tumors on the opposite pole but without clinical or histologic renal disease. The renal biopsies in the DN group were conducted to eliminate the possibility of coexistence of other kidney diseases.

2.5 | Quantitative real-time polymerase chain reaction analysis

We extracted total RNA from podocytes and frozen renal cortex utilizing TRIzol reagent and RT-qPCR kits on the basis of the manufacturer's guidelines. Complementary DNA was amplified with specific primers by means of polymerase chain reaction (PCR) for α-SMA, E-cadherin, nephrin, desmin, synaptopodin, Nox1, Nox4, Raptor, Rictor, and 18s rRNA (Table 1). Besides, we used SYBR Premix Ex Taq II to perform real-time PCR, and real-time PCR reactions were processed with the help of Agilent Mx3000P qPCR Systems (Agilent, CA).

2.6 | Western blot analysis

Radioimmunoprecipitation assay buffer was used to lyse podocytes and tissue samples, and protein was run on sodium dodecyl sulfate polyacrylamide gel electrophoresis gels before transfer to polyvinylidene fluoride membranes (Millipore, MA). Membranes were probed using primary antibodies (α-SMA, E-cadherin, nephrin, desmin, synaptopodin, Raptor, Rictor, p-S6, $p\text{-}AKT^{SER473}$ Nox1, Nox4, and β-actin) overnight at 4°C. Blots were then probed using secondary antibodies conjugated to horseradish peroxidase (HRP). Blots were scanned with the help of Odyssey Fc System (LI-COR) and band intensity was assessed using ImageJ (National Institutes of Health).

2.7 | Immunofluorescence

Briefly after culture and stimulation in six-well chamber slides, podocytes were fixed using acetone at 4°C for 10 min. The cell membrane of podocytes was punched with Triton X-100. Cells were then exposed to specific primary antibodies against α-SMA, E-cadherin, nephrin, desmin, and synaptopodin at 4°C overnight.

Podocytes were next incubated with an AF594-conjugated secondary antibody for 1 hr at 37°C. In addition, we used 4′,6-diamidino-2-phenylindole (DAPI; 1.43 μM) for nuclear staining (blue). Finally, cells were assessed via fluorescence microscopy (Olympus BX63; Olympus).

2.8 | Mitochondrial reactive oxygen species detection

MitoSox (Sigma) was used for measuring mitochondrial ROS production. After plating in six-well plates for 48 hr with appropriate stimuli, podocytes were afterwards incubated with MitoSOX (5 μM) at 37°C for 30 min. Then, podocytes were washed twice using PBS and imaged via confocal microscopy (Leica, Germany). We conducted quantitative analysis using Image-Pro Plus 6.0 (Media Cybernetics).

2.9 | Intracellular ROS detection

CM-DCHF-DA (Invitrogen) was utilized to assess the intracellular formation of ROS. Podocytes were harvested and stained in PBS containing 10 μM DCHF-DA for 30 min at 37°C. Flow cytometry (BD, NJ) was then used to assess samples.

2.10 | Tissue histology and immunohistochemistry

We utilized 4% paraformaldehyde to fix renal tissues overnight. Then kidneys were paraffin-embedded and 3-μm sections were prepared. As for paraffin-embedded tissue sections, xylene was used for deparaffinage and graded ethanol was for dehydration. Three percent hydrogen peroxide was used to deactivate internal peroxidase in 100% methanol for 30 min. Subsequently, we performed antigen retrieval at 121°C for 15 min using sodium citrate buffer (pH 6.0). Afterwards, blocked at room temperature using 10% normal goat serum for 30 min, the renal sections were then probed using primary antibodies against nephrin, synaptopodin, WT-1, Nox1, Nox4, TXNIP, Raptor, Rictor, p-S6, and p-AKT^{SER473} at 4°C overnight. Next, we washed sections before treatment with biotinylated secondary antibodies and HRP-streptavidin. We visualized labeling via 3,3-diaminobenzidine, and hematoxylin was used for counterstaining. Finally, the slides were observed using an inverted microscope (Olympus BX63; Olympus). Image-Pro Plus v6.0 was used for quantitative analyses on 10 glomeruli per kidney section. The number of WT-1–positive cells per glomerulus was counted as previously described (Shah et al., 2015).

2.11 | Statistical analysis

Data are means ± standard deviation (*SD*) for three repeat experiments. We conducted statistical analysis by means of one-way analysis of variance with GraphPad Prism 5.01 (GraphPad Software Inc.). The *t* tests were used to compare two sets of samples, with $p < 0.05$ as a threshold of statistical significance.

3 | RESULTS

3.1 | Thioredoxin-interacting protein silencing inhibits high glucose-induced epithelial-to-mesenchymal transition in podocytes

To assess how TXNIP influences podocyte HG-induced EMT, TXNIP shRNA or control plasmids were transfected into podocytes, after which they were treated with HG for 48 hr. α-SMA and desmin proteins were upregulated, while E-cadherin, nephrin, and synaptopodin were downregulated in HG group of podocytes, compared with NG group (Figure 1a–c). However, the expression of α-SMA and desmin were downregulated by TXNIP knockdown, while the protein levels of E-cadherin, nephrin, and synaptopodin showed an opposite tendency (Figure 1a–c). The results of RT-qPCR were in accordance with the western blot results (Figure 1d,e). Podocytes treated with NG or NG +mannitol group presented a spreading arborized morphology with foot processes (Figure 1f). Under HG or HG+control shRNA conditions, cells appeared to be a cobblestone or elongating morphology, and cells in HG+TXNIP shRNA plasmid group were almost similar with those under NG conditions (Figure 1f). Besides, immunofluorescent analyses of α-SMA, E-cadherin, nephrin, desmin, and synaptopodin confirmed the results of western blot analysis (Figure 1g).

3.2 | mTORC1 and mTORC2 activation was suppressed by TXNIP silencing in podocytes exposed to HG

It remains unclear whether TXNIP silencing could inhibit mammalian target of rapamycin complex 1 (mTORC1) and mammalian target of rapamycin complex 2 (mTORC2) activation induced by HG. We determined the protein expression of mTORC1 as well as mTORC2 in podocytes through western blot analysis, for the sake of exploring the activation of mTOR protein complex. By comparison, the protein levels of Raptor, p70S6K, Rictor, and p-AKT^{SER473} in podocytes of HG group were much higher than those of NG-cultured ones (Figure 2a–c). Moreover, all the alterations mentioned above were reversed by TXNIP knockdown (Figure 2a–c). The RT-qPCR results of Raptor and Rictor were in accordance with the results of the western blot (Figure 2d,e).

3.3 | Knockdown of TXNIP prevents the oxidative stress in podocytes under HG conditions

We assessed Nox1 and Nox4 expression in podocytes, which were oxidative-related proteins. Compared with NG, HG significantly upregulated Nox1 and Nox4 both at the protein and messenger RNA (mRNA) levels (Figure 3a–c). Nevertheless, TXNIP interference downregulated Nox1 and Nox4 in podocytes (Figure 3a–c). DCFH-CA was used for intracellular ROS detection in podocytes. By comparison, the ROS levels of HG-cultured podocytes were much higher than those of NG group (Figure 3d,f). Yet, knockdown of TXNIP presented an inhibitive effect on HG-induced ROS generation (Figure 3d,f). In addition, the enhanced mitochondrial ROS

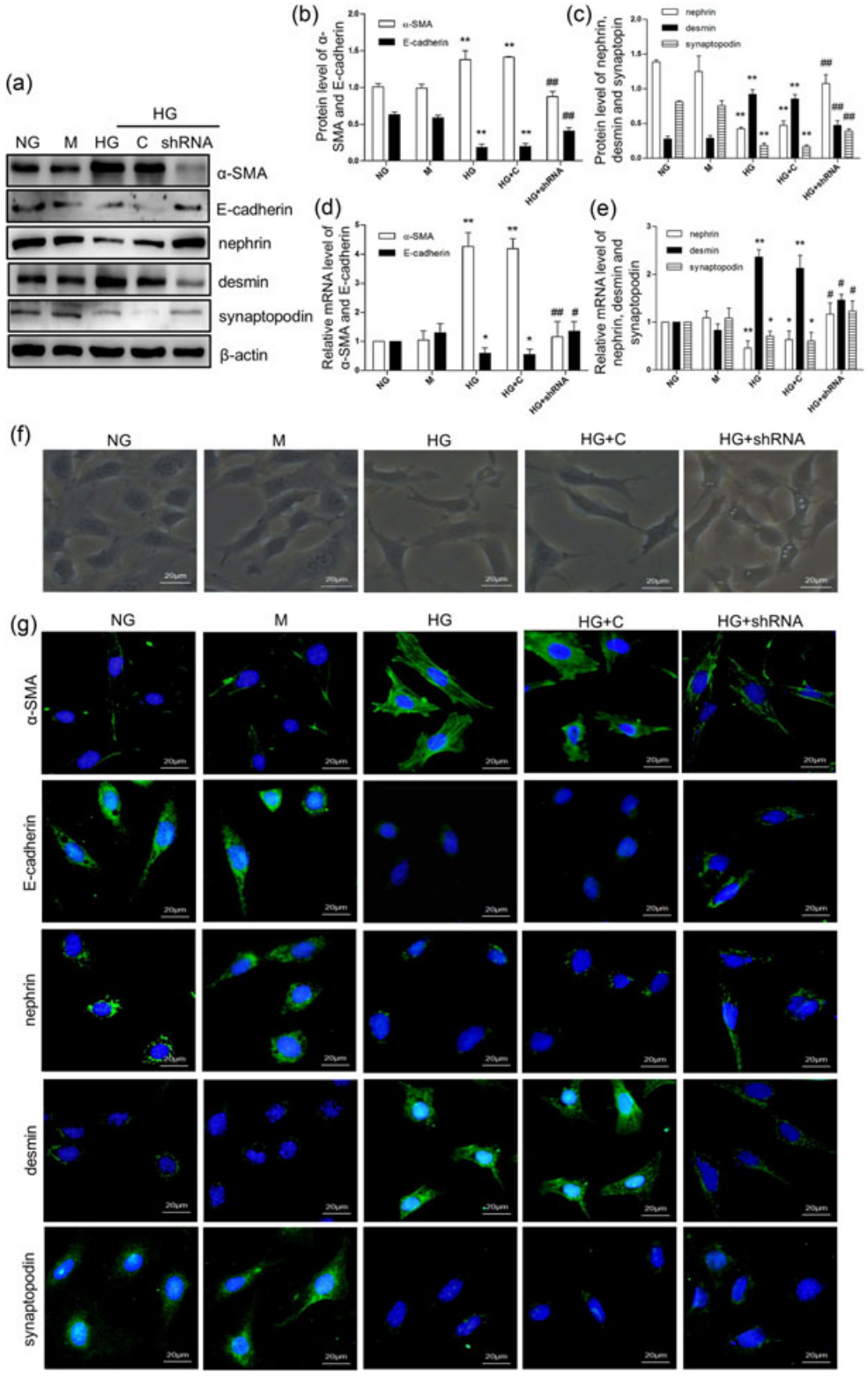

FIGURE 1 Effect of thioredoxin-interacting protein (TXNIP) silencing on high glucose (HG)-induced epithelial-to-mesenchymal transition (EMT) in podocytes. (a–c) The expression levels of α-smooth muscle actin (α-SMA), E-cadherin, desmin, nephrin, and synaptopodin protein were detected by the western blot ($n = 5$). (d,e) The messenger RNA (mRNA) levels of α-SMA, E-cadherin, desmin, nephrin, and synaptopodin were analyzed by quantitative real-time polymerase chain reaction (RT-qPCR; $n = 5$). (f) Morphological changes of podocytes cultured under different conditions were analyzed by the inverted microscope ($n = 5$). (g) The effect of TXNIP short hairpin RNA (shRNA) plasmid on the expression of α-SMA, E-cadherin, desmin, nephrin, and synaptopodin in podocytes was detected by immunofluorescence ($n = 5$). NG: 5.6 mM D-glucose; M: 5.6 mM D-glucose+24.4 mM mannitol; HG: 30 mM D-glucose; HG+C: HG+control shRNA plasmid; HG+shRNA: HG+TXNIP shRNA plasmid. Values are expressed as means ± *SD*. $^{*}p < 0.05$, $^{**}p < 0.01$ versus NG, $^{\#}p < 0.05$, $^{\#\#}p < 0.01$ versus HG+C [Color figure can be viewed at wileyonlinelibrary.com]

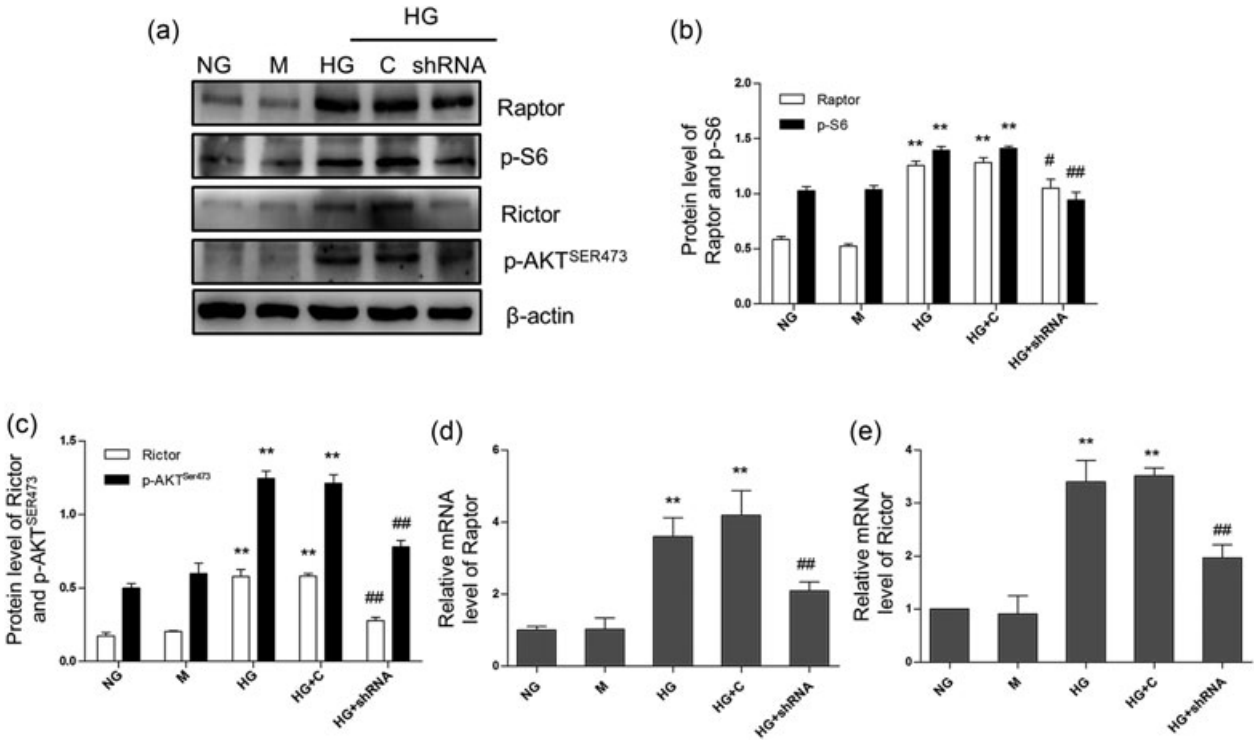

FIGURE 2 Effect of TXNIP interference on the activation of mTORC1 and mTORC2 in HG-cultured podocytes. (a–c) The protein levels of Raptor, p-S6, Rictor, and p-AKT^{SER473} were examined by western blot ($n = 5$). (d,e) The mRNA levels of Raptor and Rictor were detected by RT-qPCR ($n = 5$). NG: 5.6 mM D-glucose; M: 5.6 mM D-glucose+24.4 mM mannitol; HG: 30 mM D-glucose; HG+C: HG+control shRNA plasmid; HG +shRNA: HG+TXNIP shRNA plasmid. Values are expressed as means ± *SD*. $^{**}p < 0.01$ versus NG, $^{\#}p < 0.05$, $^{\#\#}p < 0.01$ versus HG+C. HG: high glucose; mRNA: messenger RNA; RT-qPCR: quantitative real-time polymerase chain reaction; shRNA: short hairpin RNA; TXNIP: thioredoxin-interacting protein

levels induced by HG were obviously suppressed by TXNIP shRNA transfection (Figure 3e,g).

3.4 | Inhibition of mammalian target of rapamycin represses phenotypic alterations induced by HG in podocytes

We used Raptor shRNA plasmid, Rictor shRNA plasmid, and KU-0063794 (a specific mTORC1/mTORC2 dual inhibitor) to study the function of mTOR on HG-induced phenotypic alterations in podocytes. We found that α-SMA and desmin levels in the HG group of podocytes appeared to be elevated, and this could be suppressed by Raptor shRNA plasmid, Rictor shRNA plasmid, or KU-0063794 (Figure 4a–e). Furthermore, E-cadherin, nephrin, and synaptopodin mRNA and protein seemed to lessen under HG conditions, which could be inhibited by Raptor shRNA plasmid, Rictor shRNA plasmid, and KU-0063794 (Figure 4a–e). Podocytes displayed an outstretched arborized shape with processes in NG or NG+mannitol group (Figure 4f). Podocytes presented a cobblestone or elongated shape in HG or HG+control shRNA plasmid group, and the appearances of podocytes in HG+Raptor shRNA plasmid, HG+Rictor shRNA plasmid, and HG+KU-0063794 groups were almost similar with those under NG conditions (Figure 4f). In addition, immunofluorescent detection of α-SMA, E-cadherin, nephrin, desmin, and synaptopodin verified the results of the western blot analysis (Figure 4g).

3.5 | Silencing mTOR prevents the oxidative stress in podocytes exposed to HG

We found that Nox1 and Nox4 levels were evidently upregulated under HG conditions in podocytes, compared with NG group (Figure 5a–c). However, knockdown of Raptor and Rictor, or KU-0063794 displayed an inhibitory impact on Nox1 and Nox4 (Figure 5a–c). We used DCFH-DA to detect intracellular ROS in podocytes by flow cytometry. By comparison, the ROS levels induced by HG were evidently down-regulated by knockdown of mTOR (Figure 5d,f). Besides, the enhanced mitochondrial ROS levels induced by HG were evidently decreased by transfection of Raptor shRNA, Rictor shRNA, or mTOR inhibitor KU-0063794 (Figure 5e,g).

3.6 | Antioxidant tempol or *N*-acetylcysteine shows a prohibitive effect on HG-induced EMT in podocytes

Antioxidant Tempol and NAC were utilized to explore their roles on HG-induced EMT in podocytes. Western blot results implicated that α-SMA and desmin protein were upregulated under HG conditions,

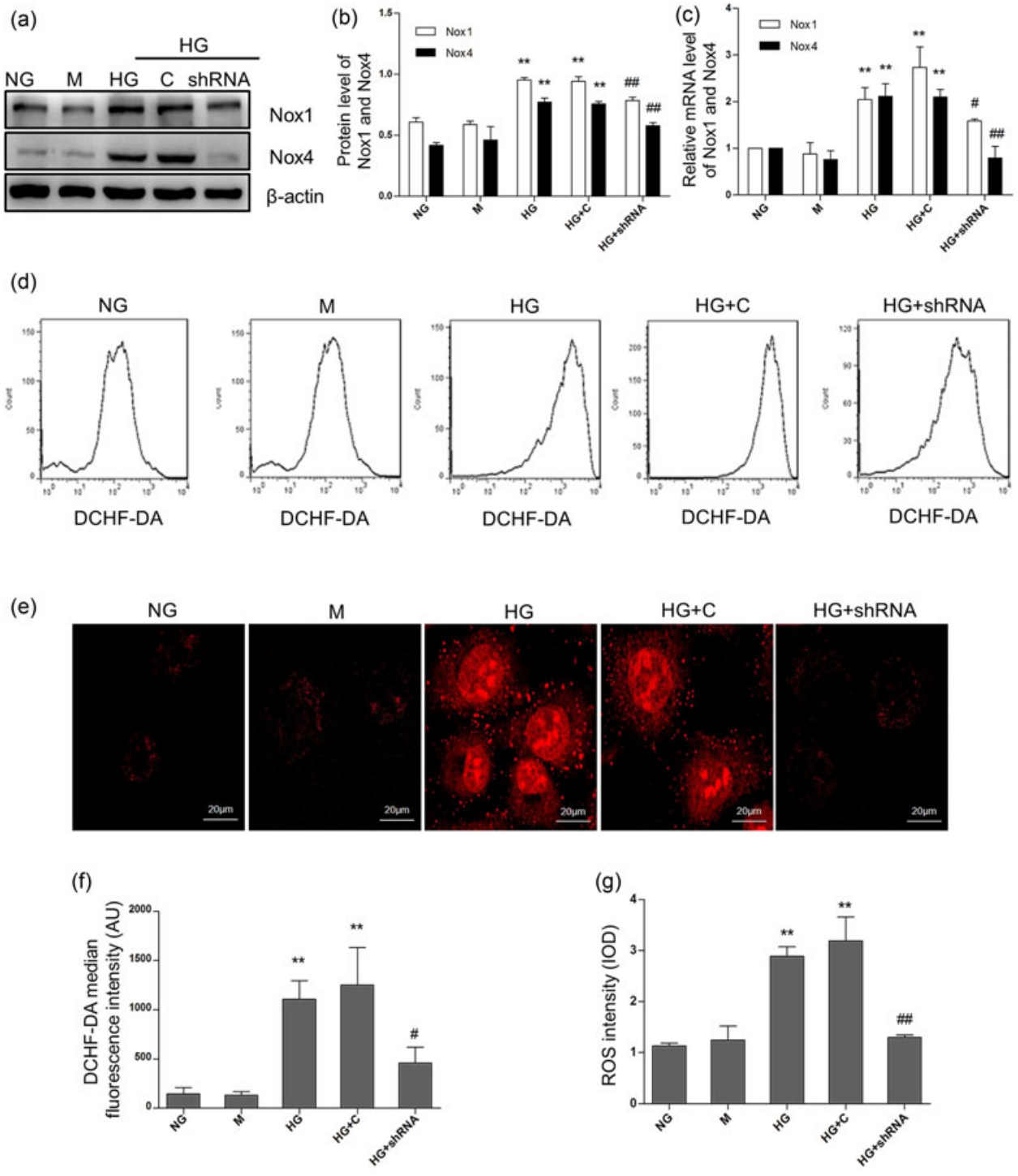

FIGURE 3 Role of TXNIP interference on the oxidative stress in HG-cultured podocytes. (a,b) The protein levels of Nox1 and Nox4 were analyzed by western blot ($n = 5$). (c) The mRNA levels of Nox1 and Nox4 were detected by RT-qPCR ($n = 5$). (d) The intracellular reactive oxygen species (ROS) were detected by flow cytometry ($n = 5$). (e) Mitochondrial ROS was detected by the confocal microscope ($n = 5$). (f) The quantitative analysis of intracellular ROS. (g) The quantitative analysis of mitochondrial ROS. NG: 5.6 mM D-glucose; M: 5.6 mM D-glucose+24.4 mM mannitol; HG: 30 mM D-glucose; HG+C: HG+control shRNA plasmid; HG+shRNA: HG+TXNIP shRNA plasmid. Values are expressed as means ± *SD*. $^{**}p < 0.01$ versus NG, $^{\#}p < 0.05$, $^{\#\#}p < 0.01$ versus HG+C. HG: high glucose; mRNA: messenger RNA; RT-qPCR: quantitative real-time polymerase chain reaction; shRNA: short hairpin RNA; TXNIP: thioredoxin-interacting protein [Color figure can be viewed at wileyonlinelibrary.com]

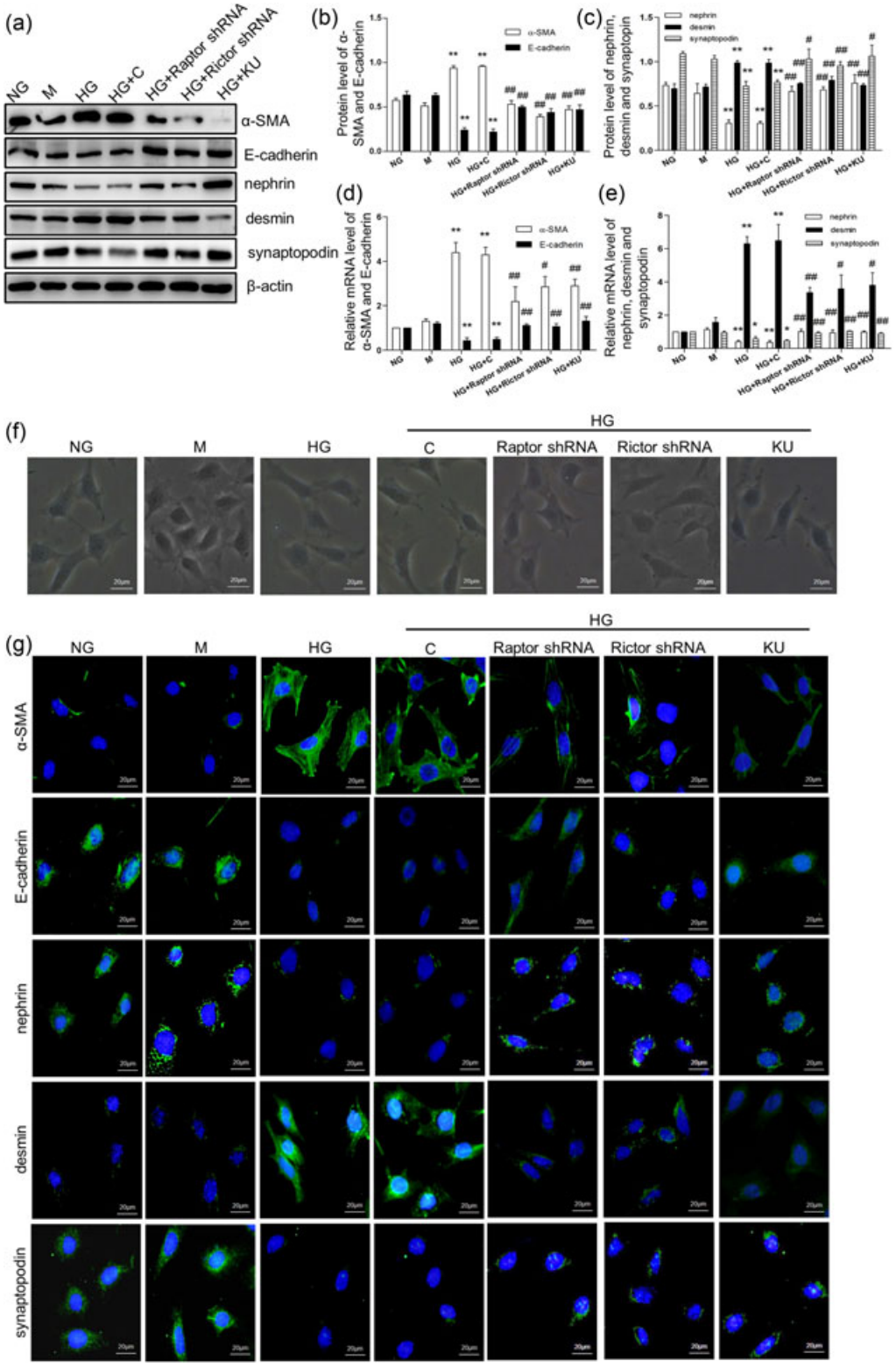

FIGURE 4 Role of mammalian target of rapamycin (mTOR) interference on HG-induced phenotypic alterations in podocytes. (a–c) The expression levels of α-SMA, E-cadherin, desmin, nephrin, and synaptopodin protein were detected by western blot ($n = 7$). (d,e) The mRNA levels of α-SMA, E-cadherin, desmin, nephrin, and synaptopodin were analyzed by RT-qPCR ($n = 7$). (f) Morphological changes of podocytes cultured under different conditions were analyzed by the inverted microscope ($n = 7$). (g) The effect of Raptor shRNA plasmid, Rictor shRNA plasmid, and KU-0063794 on the expression of α-SMA, E-cadherin, desmin, nephrin, and synaptopodin in podocytes was detected by immunofluorescence ($n = 7$). NG: 5.6 mM D-glucose; M: 5.6 mM D-glucose+24.4 mM mannitol; HG: 30 mM D-glucose; HG+C: HG+control shRNA plasmid; HG+Raptor: HG+Raptor shRNA plasmid; HG+Rictor: HG+Rictor shRNA plasmid; HG+KU: HG+KU-0063794 (1 μM). Values are expressed as means ± *SD*. $^{*}p < 0.05$, $^{**}p < 0.01$ versus NG, $^{\#}p < 0.05$, $^{\#\#}p < 0.01$ versus HG+C. α-SMA: α-smooth muscle actin; HG: high glucose; mRNA: messenger RNA; RT-qPCR: quantitative real-time polymerase chain reaction; shRNA: short hairpin RNA [Color figure can be viewed at wileyonlinelibrary.com]

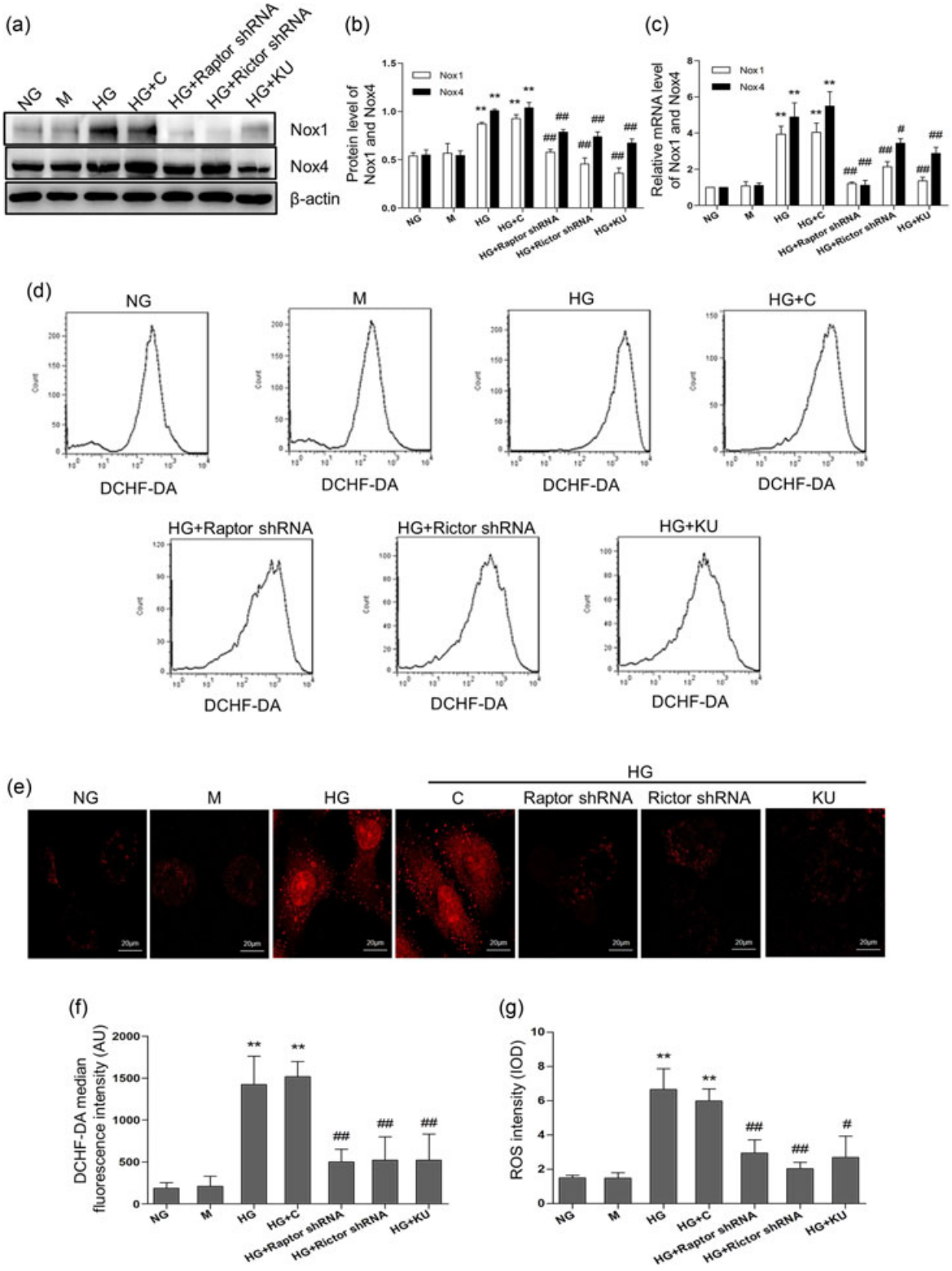

FIGURE 5 Role of knockdown of mTOR on the oxidative stress in HG-cultured podocytes. (a,b) The protein levels of Nox1 and Nox4 were detected by the western blot ($n = 7$). (c) The mRNA levels of Nox1 and Nox4 were detected by RT-qPCR ($n = 7$). (d) The intracellular ROS were detected by flow cytometry ($n = 7$). (e) Mitochondrial ROS was detected by the confocal microscope ($n = 7$). (f) The quantitative analysis of intracellular ROS. (g) The quantitative analysis of mitochondrial ROS. NG: 5.6 mM D-glucose; M: 5.6 mM D-glucose+24.4 mM mannitol; HG: 30 mM D-glucose; HG+C: HG+control shRNA plasmid; HG+Raptor: HG+Raptor shRNA plasmid; HG+Rictor: HG+Rictor shRNA plasmid; HG +KU: HG+KU-0063794 (1 μM). Values are expressed as means ± *SD*. $^{**}p < 0.01$ versus NG, $^{\#}p < 0.05$, $^{\#\#}p < 0.01$ versus HG+C. HG: high glucose; mRNA: messenger RNA; mTOR: mammalian target of rapamycin; ROS: reactive oxygen species; RT-qPCR: quantitative real-time polymerase chain reaction; shRNA: short hairpin RNA [Color figure can be viewed at wileyonlinelibrary.com]

while E-cadherin, nephrin, and synaptopodin were downregulated (Figure 6a–c). Whereas, these alterations could be inhibited by Tempol or NAC (Figure 6a–c). RT-qPCR results were in line with the results of the western blot (Figure 6d,e). Podocytes seemed to present a spreading arborized morphology with processes in NG or NG +mannitol group (Figure 6f). When under HG conditions, however, podocytes tended to display a cobblestone or elongated morphology, and podocytes in HG+Tempol and HG+NAC groups were similar with those under NG conditions (Figure 6f). Besides, immunofluorescence detection of α-SMA, E-cadherin, nephrin, desmin, and synaptopodin confirmed the results of the western blot (Figure 6g).

3.7 | Lack of TXNIP restrains glomerular manifestations in diabetic mice

To assess the function of TXNIP in DN, STZ was utilized to induce type 1 diabetes in WT and TXNIP$^{-/-}$ (KO) mice for 16 weeks. Biochemical characteristics and renal measures of mice, including blood glucose, kidney weight, body weight, kidney/body weight, Upro, Scr, BUN, and TG, are shown in Table 2. Body weight was lower in both diabetic groups relative to WT animals (Table 2). Kidney/body weight ratio appeared to be higher in diabetic WT mice, which was lower in diabetic TXNIP KO mice (Table 2). The amount of Upro obviously ascended in the urine of diabetic WT mice, which showed a downtrend in diabetic TKO mice (Table 2). By comparison to the nondiabetic ones, the levels of Scr, BUN, and TG in the serum of diabetic WT mice were much higher, which reduced in that of diabetic TXNIP KO mice (Table 2). These findings indicated that TXNIP deficiency protected the kidneys from renal impairment of DN.

3.8 | Lack of TXNIP reverses phenotypic alterations of podocytes and reduction of podocyte number in diabetic mice

Next, we assessed the importance of TXNIP for phenotypic alterations of podocytes in diabetic mice. Compared with nondiabetic controls, the nephrin and synaptopodin gene and protein expression presented a downtrend in diabetic WT mice, which increased in diabetic TKO mice (Figure 7a–c). In addition, immunohistochemistry results indicated that the expression of nephrin and synaptopodin tended to be reduced markedly in diabetic WT mice, which reversed in diabetic TKO ones (Figure 7d,f). Since podocytes function in the glomerular filtration barrier, the loss of podocytes signals progression to advanced disease (Dronavalli et al., 2008; Rask-Madsen & King, 2013). Thus, the podocyte number was examined via Wilms' tumor antigen-1 (WT-1) staining, as this transcription factor is only known to be expressed in podocytes (Quaggin & Kreidberg, 2008). There was an obvious reduction in podocyte number in diabetic WT mice, whereas numbers in diabetic TXNIP KO mice were not substantially decreased (Figure 7e,g).

3.9 | TXNIP deficiency inhibits diabetes-induced oxidative stress

The expression of 8-OHdG was detected by enzyme-linked immunosorbent assay. Relative to WT mice, 8-OHdG expression was markedly elevated in diabetic WT mice, but reduced in the TKO mice (Table 2). In addition, Nox1 and Nox4 protein levels in diabetic WT mice were evidently upregulated than those of nondiabetic controls, and the opposite was true in TXNIP KO mice (Figure 8a,b). Gene expression analyses were consistent with the western blot analysis (Figure 8c). In addition, we detected Nox1 and Nox4 expression in podocytes of mice by immunohistochemistry. Nox1 and Nox4 expression was augmented in diabetic WT mice, while the opposite was true in diabetic TXNIP KO mice (Figure 8d–f).

3.10 | TXNIP deficiency suppresses mTORC1 and mTORC2 activation in glomeruli of diabetic mice

To be more profound, we explored the role of TXNIP on the activation of mTORC1 and mTORC2 in the glomeruli of STZ-induced diabetic mice. Results of immunohistochemistry showed that the expression of Raptor and p-S6 markedly augmented in the glomeruli of diabetic WT mice in comparison to WT ones, however, this was reversed in the glomeruli of diabetic TKO mice (Figure 9a,b). Moreover, in comparison to WT mice, the expression of Rictor and p-AKT^{SER473} elevated in the glomeruli of WT mice, which was suppressed in the glomeruli of TXNIP KO mice (Figure 9a,c).

3.11 | The expression of TXNIP, mTOR pathway, Nox1, and Nox4 could be detected in the glomeruli of patients with diabetic nephropathy

We conducted immunohistochemistry utilizing renal biopsy tissues of patients with DN and normal control patients for better elucidating the expression of TXNIP, mTOR pathway, Nox1, and Nox4 in patients with DN . Relative to normal control patients, TXNIP expression was evidently augmented in the glomeruli of patients with DN (Figure 10a). Besides, the expression of Raptor, Rictor, p-S6, and p-AKT^{SER473} remarkably increased in the glomeruli of patients with DN compared with normal control patients (Figure 10a). Also, compared with normal control patients, Nox1 and Nox4 were more highly expressed in the glomeruli of patients with DN (Figure 10a).

4 | DISCUSSION

DN is a serious health problem responsible for roughly 1/3rd of end-stage renal disease cases (Dronavalli et al., 2008; Molitch et al., 2004). Among the various derangements relevant with diabetes, oxidative stress is also known to be a key mediator of DN pathogenesis (Sifuentes-Franco, Padilla-Tejeda, Carrillo-Ibarra, & Miranda-Diaz, 2018), and studies have suggested that protein TXNIP is linked to DN pathogenesis as well (Advani et al., 2009; Shah et al., 2013; Tan,

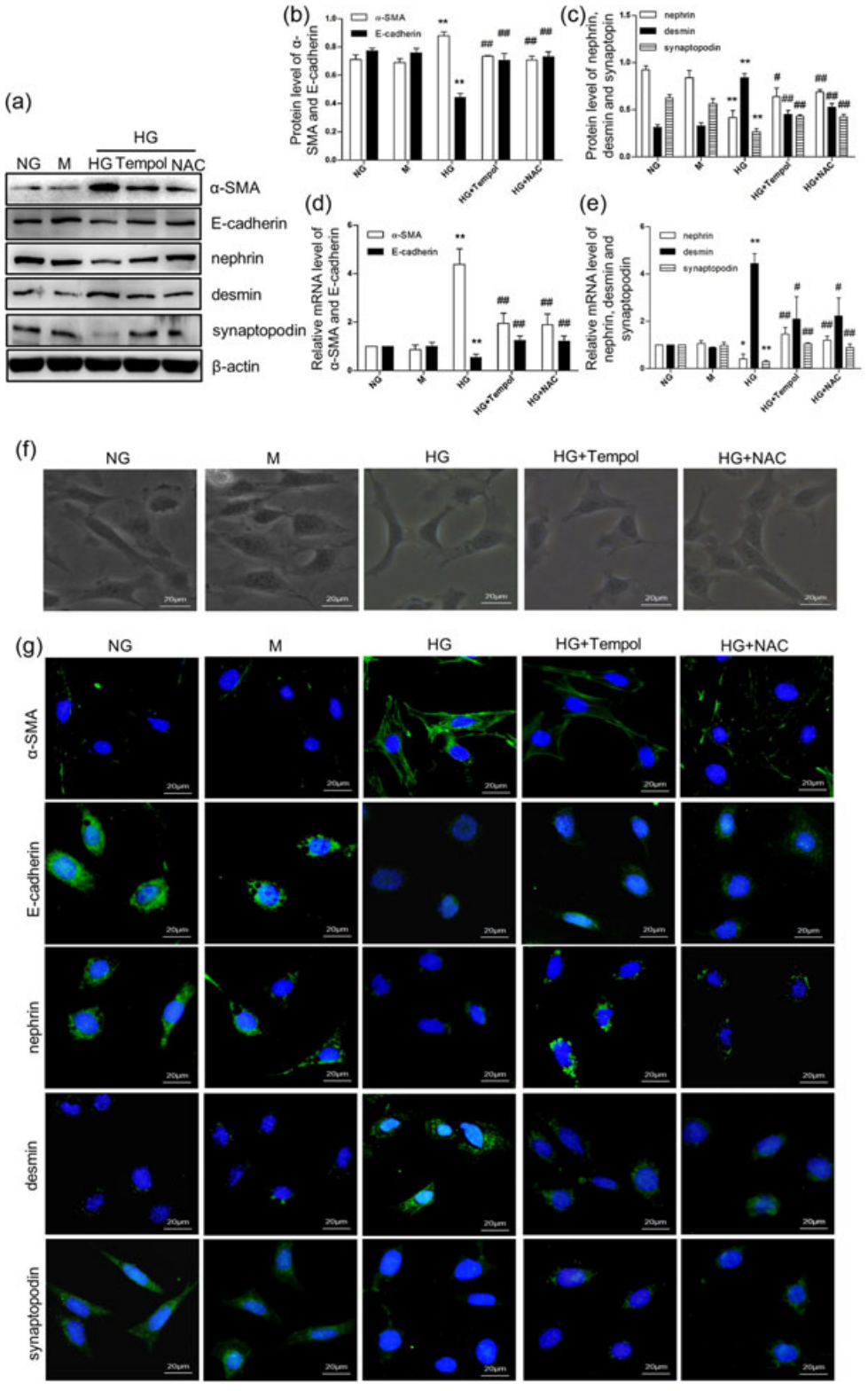

FIGURE 6 Effect of Tempol and *N*-acetylcysteine (NAC) on HG-induced phenotypic alterations in podocytes. (a–c) The expression levels of α-SMA, E-cadherin, desmin, nephrin, and synaptopodin protein were detected by western blot ($n = 5$). (d,e) The mRNA levels of α-SMA, E-cadherin, desmin, nephrin, and synaptopodin were analyzed by RT-qPCR ($n = 5$). (f) Morphological changes of podocytes cultured under different conditions were analyzed by the inverted microscope ($n = 5$). (g) The effect of Tempol and NAC on the expression of α-SMA, E-cadherin, desmin, nephrin, and synaptopodin in podocytes was detected by immunofluorescence ($n = 5$). NG: 5.6 mM D-glucose; M: 5.6 mM D-glucose+24.4 mM mannitol; HG: 30 mM D-glucose; HG+Tempol: HG+Tempol (1 mM); HG+NAC: HG+NAC (5 mM). Values are expressed as means ± *SD*. $^{*}p < 0.05$, $^{**}p < 0.01$ versus NG, $^{\#}p < 0.05$, $^{\#\#}p < 0.01$ versus HG+C. α-SMA: α-smooth muscle actin; HG: high glucose; mRNA: messenger RNA; RT-qPCR: quantitative real-time polymerase chain reaction [Color figure can be viewed at wileyonlinelibrary.com]

TABLE 2 Physical and metabolic parameters among different groups ($\bar{X}$±S)

Parameters	WT	TKO	WT+DM	TKO+DM
Blood glucose (mmol/L)	6.63 ± 1.63	6.77 ± 0.99	32.3 ± 1.73**	17.1 ± 1.65**
Body weight (g)	30.7 ± 0.95	28.1 ± 0.62	23.33 ± 0.91**	24.7 ± 1.66
Kidney weight (g)	0.38 ± 0.02	0.36 ± 0.02	0.43 ± 0.04	0.41 ± 0.06
Kidney/Body weight (mg/g)	12.2 ± 1.01	12.92 ± 0.06	19.57 ± 1.35**	15.46 ± 1.38**
Upro (mg/24 hr)	5.343 ± 0.56	9.531 ± 1.69	43.52 ± 3.87**	18.84 ± 1.32**
Scr (μmol/L)	32.68 ± 1.81	33.65 ± 2.94	108.6 ± 5.96**	58.31 ± 2.73**
BUN (mmol/L)	11.34 ± 1.21	13.77 ± 1.73	42.35 ± 1.57**	16.71 ± 2.22**
TG (mg/dL)	17.35 ± 2.35	16.66 ± 2.84	186.6 ± 5.93**	105.7 ± 6.40**
8-OHdG (ng/mL)	22.26 ± 3.23	23.97 ± 1.59	57.67 ± 2.18**	38.24 ± 2.50**

Note. 8-OHdG: 8-hydroxydeoxyguanosine; BUN: blood urea nitrogen; Scr: serum creatinine; TG: triglyceride; TKO: TXNIP knockout; Upro: urinary protein; WT: wild type

*$p < 0.05$.

**$p < 0.01$, versus WT group.

#$p < 0.05$.

##$p < 0.01$, versus WT+DM group.

Zhang, Cox, Kelly, & Qi, 2011; J. Wu et al., 2013). As such, we utilized human renal biopsies to explore the expression of TXNIP in patients with DN and found that TXNIP expression obviously augmented in glomeruli of patients with DN compared with normal control patients. Shah et al. (2015) demonstrated that TXNIP deficiency attenuated renal injury, extracellular matrix accumulation, and renal fibrosis induced by diabetes. We also used the mouse model of TXNIP deficiency, $TXNIP^{-/-}$ (TKO) mice. We found that renal measures like Upro, Scr, TG, and BUN, presented to increase in WT mice with diabetes. However, these alterations were reversed in diabetic TKO mice, which indicated that diabetic renal lesions were attenuated by TXNIP deficiency. In addition, defective glomerular function is a key driver of DN, and podocytes are a very vulnerable component of this system. Shah et al (2015) also reported that TXNIP deficiency could reduce podocyte loss. In the present study, immunohistochemical staining for WT-1 suggested the reduction in podocyte number was reversed in diabetic TXNIP KO mice, implicating that TXNIP deficiency may play a key effect in attenuating podocyte loss in DN.

The specific pancreatic islet β-cell injury is unique to type 1 diabetes (Mathis, Vence, & Benoist, 2001). STZ could directly damage pancreatic islet β-cells, thus leading to diabetes mellitus. One hypothesis demonstrated that TXNIP might be a glucose-induced proapoptotic factor of β-cell using isolated islets from TKO mice (Chen, Saxena, Mungrue, Lusis, & Shalev, 2008). Moreover, this group showed that lack of TXNIP could inhibit β-cell apoptosis, increase β-cell mass, and improve insulin sensitivity in the context of generalized TXNIP deficiency, thus protecting against STZ-induced diabetes (Chen, Hui, et al., 2008). Interestingly, we found that the blood glucose level of diabetic TKO mice was much lower than that of diabetic WT ones, indicating TXNIP deficiency might play an important role in reducing blood glucose level in DN. Besides, podocyte injury is considered to be crucial in the processes of various primary and secondary glomerular diseases. Under normal conditions, podocytes could adhere to GBM to maintain their normal structure and function through α3β1-integrin. Hyperglycemia could suppress the expression of α3β1-integrin, thus leading to podocyte detachment (Kitsiou et al., 2003). Susztak, Raff, Schiffer, and Böttinger (2006) indicated that glucose-induced ROS initiated podocyte apoptosis and depletion both in vivo and in vitro. In our study, the phenotypic alterations of podocytes could be alleviated in diabetic TKO mice, thereby suggesting that lower blood glucose may alleviate podocyte injury in TKO mice with diabetes.

The phenotypic alteration of podocytes refers to that, differentiated podocytes may lose their epithelial specificity and undergo a phenotypic transformation that brings about the matrix-producing fibroblasts and myofibroblasts, mediating postinjury tissue fibrogenesis (Liu, 2010). Several in vivo and in vitro studies have implicated that HG may cause the phenotypic alterations of podocytes, thus leading to structural and functional impairment of podocytes (Guo, Yang, Qiao, & Liu, 2016; Ling, Chen et al., 2018; Ling, Tan et al., 2018). In our study, we demonstrated that HG could enhance the expression levels of α-SMA and desmin, and reduce the levels of E-cadherin, synaptopodin, and nephrin, thus inducing phenotypic alterations in cultured mouse podocytes. Meanwhile, the phenotypic conversions were observed in diabetic WT mice, too. Nevertheless, these phenotypic alterations could be ameliorated in diabetic TKO mice, demonstrating the role of TXNIP deficiency on improving the phenotypic alterations of podocytes in DN.

Excess mitochondrial ROS production in response to HG levels has been suggested to be a key driver of diabetic complications including DN (Nishikawa et al., 2000; Giacco & Brownlee, 2010). Resultant redox alterations can inhibit glyceraldehyde-3-phosphate dehydrogenase, ultimately leading to enhanced glucose metabolism via multiple mechanisms, leading to its toxicity (Shah et al., 2015). It is reported that ROS mediated EMT induced by HG, TGF-β1, and Ang II in renal tubular epithelial cells (Lee et al., 2013; Wei et al., 2013). In our study, Tempol and NAC were utilized to explore the impact of ROS on HG-induced EMT in podocytes. As a result, these antioxidants could inhibit HG-induced EMT in podocytes, indicating

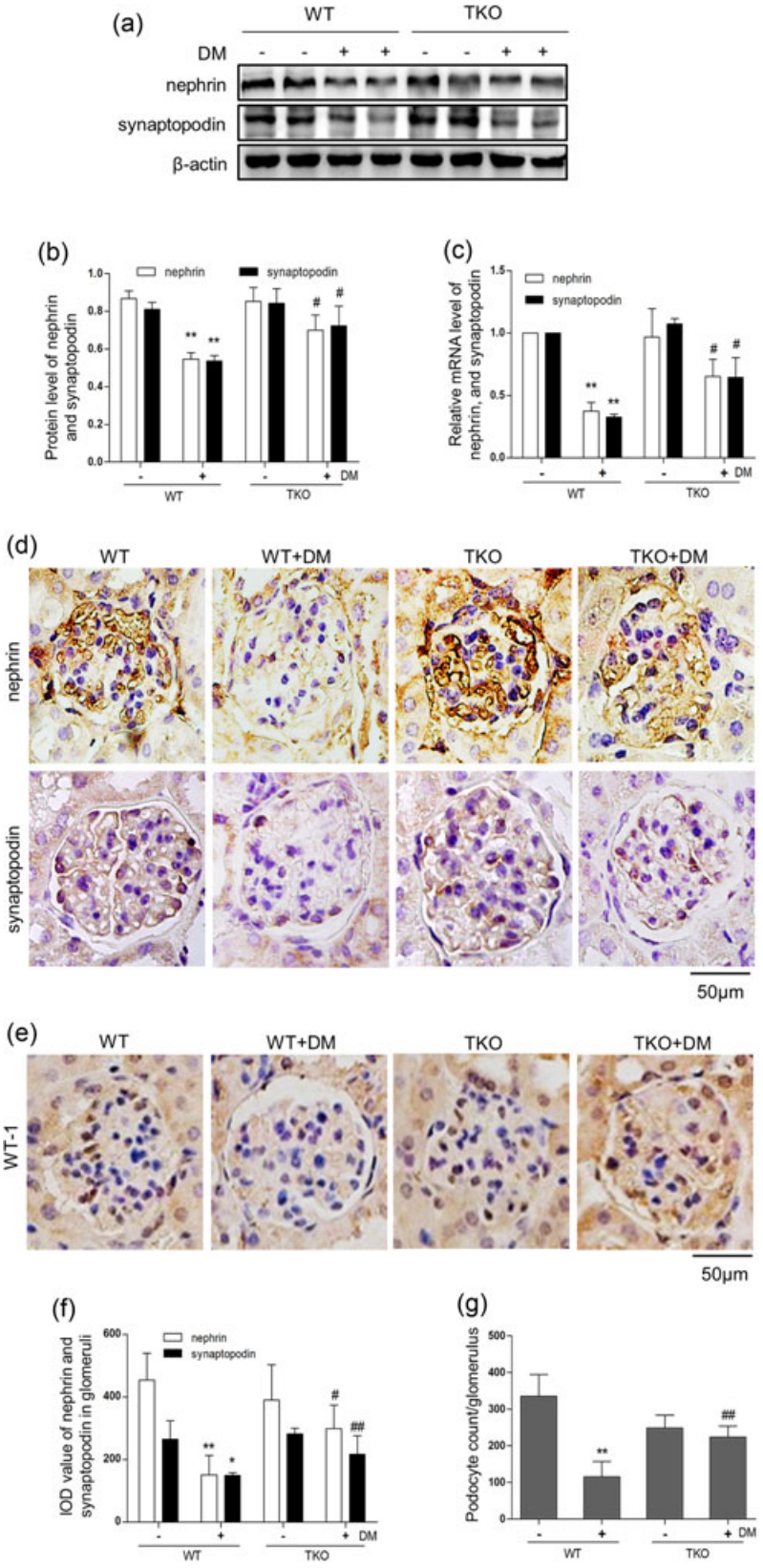

FIGURE 7 Lack of TXNIP reverses phenotypic alterations of podocytes and reduction of podocyte number in diabetic mice. (a,b) The expression levels of nephrin and synaptopodin protein were detected by western blot ($n = 4$). (c) The mRNA levels of nephrin and synaptopodin were analyzed by RT-qPCR ($n = 4$). (d) The immunohistochemistry of kidney sections for nephrin and synaptopodin from control, diabetic wild type (WT) and TXNIP KO mice. (e) Immunohistochemistry of kidney tissues with WT-1 antibody. $N = 3$. (f) The IOD value of nephrin and synaptopodin in glomeruli from control, diabetic WT, and TXNIP KO mice. (g) The number of WT-1–positive cells per glomerulus in mice. All values are expressed as mean ± *SD*. $^{**}p < 0.01$ versus nondiabetic WT mice, $^{\#}p < 0.05$, $^{\#\#}p < 0.01$ versus diabetic WT mice. mRNA: messenger RNA; RT-qPCR: quantitative real-time polymerase chain reaction; TXNIP: thioredoxin-interacting protein [Color figure can be viewed at wileyonlinelibrary.com]

the impact of ROS on HG-induced EMT. Furthermore, our previous studies proved that TXNIP deficiency may suppress HG-induced ROS in mouse mesangial cells and human renal tubular epithelial cells (Shi et al., 2011; Wei et al., 2013). Besides, we found that Nox1 and Nox4 expression markedly rose in the glomeruli of patients with DN in contrast to normal control patients, TXNIP shRNA inhibited the production of ROS as well as the levels of Nox1 and Nox4 in HG-treated podocytes, and the expression of Nox1 and Nox4 were

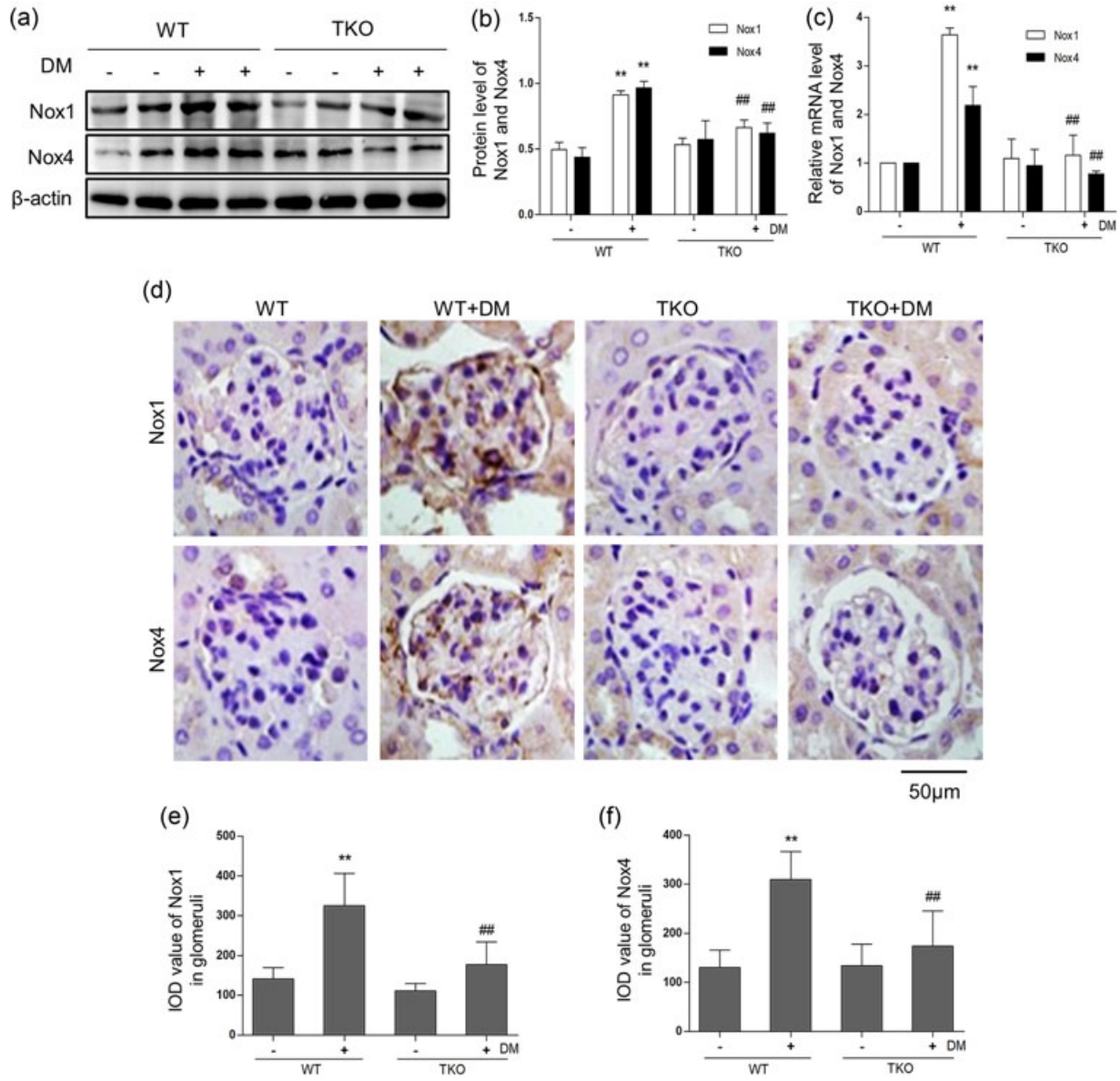

FIGURE 8 TXNIP deficiency inhibits diabetes-induced oxidative stress. (a,b) The protein levels of Nox1 and Nox4 were analyzed by western blot ($n = 4$). (c) The mRNA levels of Nox1 and Nox4 were detected by RT-qPCR ($n = 4$). (d) Immunohistochemistry of kidney tissues with Nox1 and Nox4 antibody. (e,f) The IOD value of Nox1 and Nox4 in glomeruli in control, diabetic WT and TXNIP KO mice. $N = 3$. All values are expressed as mean ± *SD*. $^{**}p < 0.01$ versus nondiabetic WT mice, $^{\#\#}p < 0.01$ versus diabetic WT mice. mRNA: messenger RNA; RT-qPCR: quantitative real-time polymerase chain reaction; TXNIP: thioredoxin-interacting protein; WT: wild type [Color figure can be viewed at wileyonlinelibrary.com]

downregulated in diabetic TKO mice, suggesting that lack of TXNIP might inhibit the generation of ROS in DN.

The molecular mechanism of DN is poorly understood and remains to be elucidated. It has been documented that mTOR is involved in DN (Eid et al., 2013; Godel et al., 2011; Inoki et al., 2011), and the activation of mTOR pathway is associated with TXNIP (Huang et al., 2014). Studies also indicate that HG-induced mTOR phosphorylation could be alleviated by TXNIP siRNA transfection in renal tubular cells (Inoki, 2014; Tanaka et al., 2012). In our study, immunohistochemistry results revealed that the expression of Raptor, Rictor, p-S6, and p-AKT^{SER473} was significantly upregulated in the glomeruli of patients with DN in comparison to normal control patients, and the activation of mTOR (both mTORC1 and mTORC2) was significantly restrained in HG-cultured podocytes transfected with TXNIP shRNA and the glomeruli of diabetic TXNIP KO mice. Several reports have implicated that mTOR signal pathway is linked with HG-induced EMT in renal tubular cells (Gong & Hou, 2016; Habib, 2013; Xu et al., 2015), thus, we used Raptor shRNA, Rictor shRNA, and mTOR inhibitor KU-0063794 to investigate the role of mTOR on phenotypic alterations of podocytes in DN. We found that HG-induced EMT in cultured podocytes was remarkably suppressed via mTOR inhibition. In addition, inhibition of mTOR could also reduce the generation of ROS, along with the expression of Nox1 and Nox4 in podocytes under HG conditions.

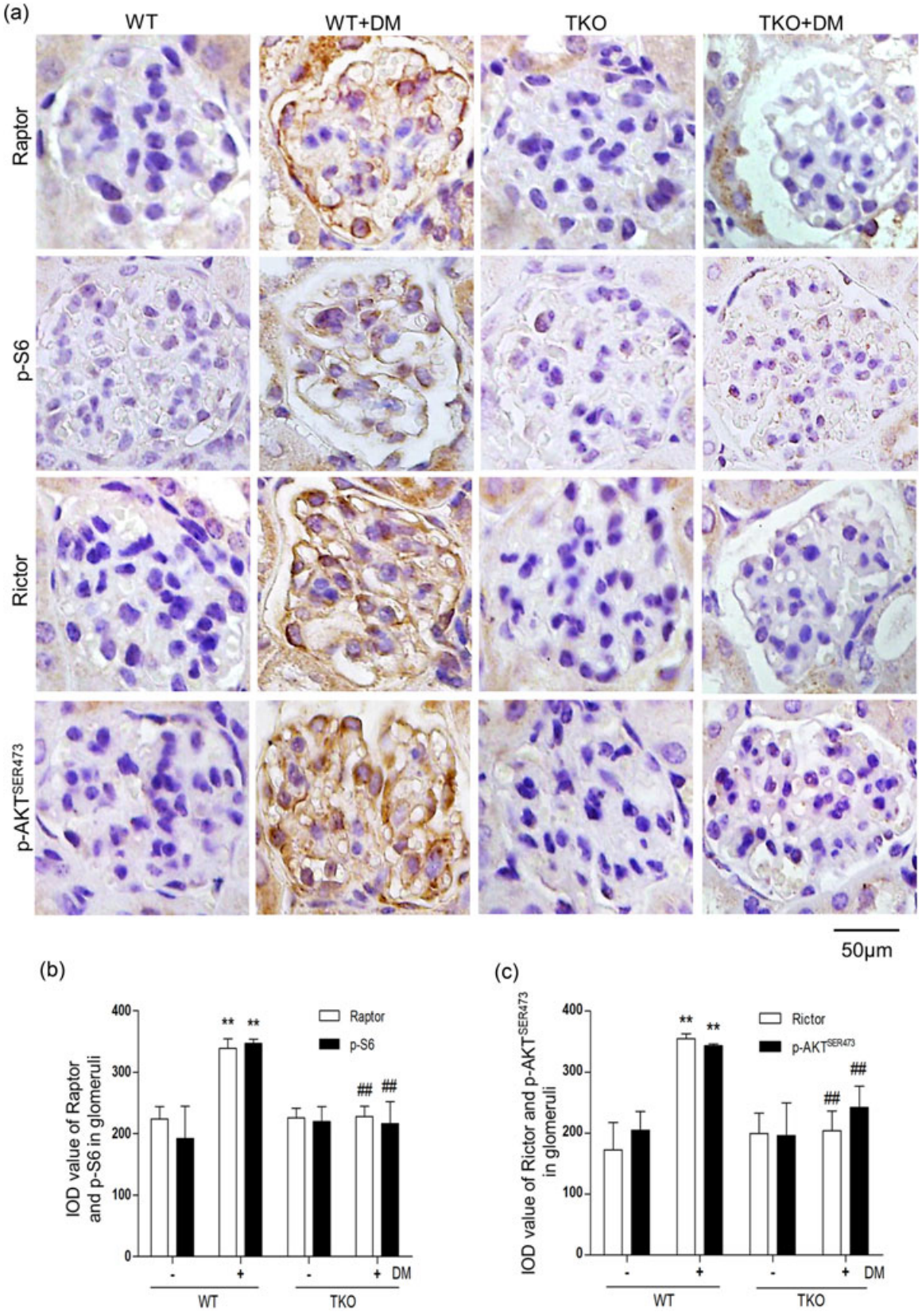

FIGURE 9 TXNIP deficiency could inhibit the activation of mammalian target of rapamycin complex 1 and mammalian target of rapamycin complex 2 in the glomeruli of streptozotocin-induced diabetic mice. (a) Immunohistochemistry of renal tissues with Raptor, p-S6, Rictor, and p-AKT^{SER473} antibody. (b,c) The IOD value of Raptor, p-S6, Rictor, and p-AKT^{SER473} in glomeruli in control, diabetic WT, and TXNIP KO mice. $N = 3$. All values are expressed as mean ± *SD*. $^{**}p < 0.01$ versus nondiabetic WT mice, $^{\#\#}p < 0.01$ versus diabetic WT mice. TXNIP: thioredoxin-interacting protein; WT: wild type [Color figure can be viewed at wileyonlinelibrary.com]

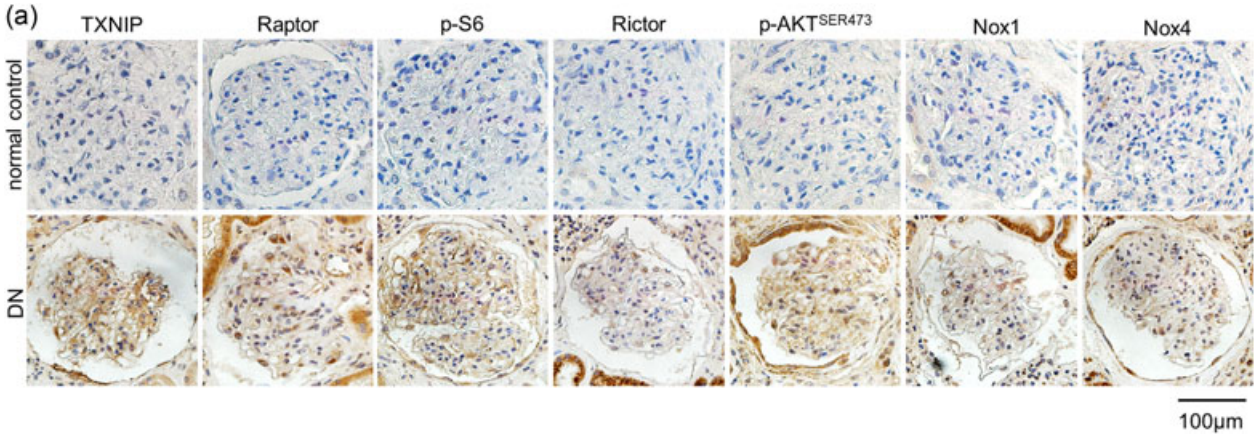

FIGURE 10 The expression of TXNIP, mTOR activation, Nox1, and Nox4 could be detected in patients with diabetic nephropathy (DN). (a) The expression of TXNIP, Raptor, Rictor, p-S6, p-AKT^{SER473}, Nox1, and Nox4 was examined by immunohistochemistry in renal biopsy tissues of 12 samples from patients with type 2 diabetes and biopsy-proven DN and four samples from normal control patients. mTOR: mammalian target of rapamycin; TXNIP: thioredoxin-interacting protein [Color figure can be viewed at wileyonlinelibrary.com]

Taken together, TXNIP, Nox1, and Nox4 expression along with mTOR activation could be detected in renal biopsy tissue glomeruli from patients with DN. In vivo data verify that TKO mice were protected from renal impairment, podocyte loss, podocyte phenotypic alterations, oxidative stress, and mTOR activation in glomeruli in STZ-induced diabetes. Besides, in vitro data indicate that TXNIP interference could inhibit HG-induced EMT, oxidative stress, and the activation of mTOR. Meanwhile, mTOR inhibition may suppress HG-induced EMT and oxidative stress, and Tempol and NAC could inhibit HG-induced EMT as well. Therefore, our results recognize TXNIP as a promising therapeutic target for DN.

FUNDING INFORMATION

The National Natural Science Foundation of China (Nos. 81270804 and 81470966), China Postdoctoral Science Foundation (No. 2014M561199), and Hebei Human Resources and Social Security Department Project (No. A2017003080) funded this study.

ORCID

Shan Song http://orcid.org/0000-0002-2841-2213

REFERENCES

Advani, A., Gilbert, R. E., Thai, K., Gow, R. M., Langham, R. G., Cox, A. J., … Kelly, D. J. (2009). Expression, localization, and function of the thioredoxin system in diabetic nephropathy. *Journal of the American Society of Nephrology*, *20*(4), 730–741.

Benzing, T. (2004). Signaling at the slit diaphragm. *Journal of the American Society of Nephrology*, *15*(6), 1382–1391.

Chen, J., Saxena, G., Mungrue, I. N., Lusis, A. J., & Shalev, A. (2008). Thioredoxin-interacting protein: A critical link between glucose toxicity and beta-cell apoptosis. *Diabetes*, *57*(4), 938–944.

Chen, J., Hui, S. T., Couto, F. M., Mungrue, I. N., Davis, D. B., Attie, A. D., … Shalev, A. (2008). Thioredoxin-interacting protein deficiency induces Akt/Bcl-xL signaling and pancreatic beta-cell mass and protects against diabetes. *FASEB Journal*, *22*(10), 3581–3594.

Cheng, D. W., Jiang, Y., Shalev, A., Kowluru, R., Crook, E. D., & Singh, L. P. (2006). An analysis of high glucose and glucosamine-induced gene expression and oxidative stress in renal mesangial cells. *Archives of Physiology and Biochemistry*, *112*(4-5), 189–218.

Dann, S. G., Selvaraj, A., & Thomas, G. (2007). mTOR Complex1-S6K1 signaling: At the crossroads of obesity, diabetes and cancer. *Trends in Molecular Medicine*, *13*(6), 252–259.

Dronavalli, S., Duka, I., & Bakris, G. L. (2008). The pathogenesis of diabetic nephropathy. *Nature Clinical Practice. Endocrinology & Metabolism*, *4*(8), 444–452.

Eid, A. A., Ford, B. M., Bhandary, B., de Cassia Cavaglieri, R., Block, K., Barnes, J. L., … Abboud, H. E. (2013). Mammalian target of rapamycin regulates Nox4-mediated podocyte depletion in diabetic renal injury. *Diabetes*, *62*(8), 2935–2947.

Giacco, F., & Brownlee, M. (2010). Oxidative stress and diabetic complications. *Circulation Research*, *107*(9), 1058–1070.

Gödel, M., Hartleben, B., Herbach, N., Liu, S., Zschiedrich, S., Lu, S., … Huber, T. B. (2011). Role of mTOR in podocyte function and diabetic nephropathy in humans and mice. *Journal of Clinical Investigation*, *121*(6), 2197–2209.

Gong, Q., & Hou, F. (2016). Silencing of angiotensin II type-1 receptor inhibits high glucose-induced epithelial-mesenchymal transition in human renal proximal tubular epithelial cells via inactivation of mTOR/p70S6K signaling pathway. *Biochemical and Biophysical Research Communications*, *469*(2), 183–188.

Guo, J., Yang, L., Qiao, Y., & Liu, Z. (2016). Glycogen synthase kinase-3β is required for epithelialmesenchymal transition and barrier dysfunction in mouse podocytes under high glucose conditions. *Molecular Medicine Reports*, *14*(5), 4091–4098.

Habib, S. L. (2013). Alterations in tubular epithelial cells in diabetic nephropathy. *Journal of Nephrology*, *26*(5), 865–869.

Huang, C., Lin, M. Z., Cheng, D., Braet, F., Pollock, C. A., & Chen, X. M. (2014). Thioredoxin-interacting protein mediates dysfunction of tubular autophagy in diabetic kidneys through inhibiting autophagic flux. *Laboratory Investigation*, *94*(3), 309–320.

Inoki, K. (2014). mTOR signaling in autophagy regulation in the kidney. *Seminars in Nephrology*, *34*(1), 2–8.

Inoki, K., Mori, H., Wang, J., Suzuki, T., Hong, S., Yoshida, S., … Guan, K. L. (2011). mTORC1 activation in podocytes is a critical step in the development of diabetic nephropathy in mice. *Journal of Clinical Investigation*, *121*(6), 2181–2196.

Iwano, M., Plieth, D., Danoff, T. M., Xue, C., Okada, H., & Neilson, E. G. (2002). Evidence that fibroblasts derive from epithelium during tissue fibrosis. *Journal of Clinical Investigation*, *110*(3), 341–350.

Kitsiou, P. V., Tzinia, A. K., Stetler-Stevenson, W. G., Michael, A. F., Fan, W. W., Zhou, B., & Tsilibary, E. C. (2003). Glucose-induced changes in integrins and matrix-related functions in cultured human glomerular epithelial cells. *American Journal of Physiology. Renal Physiology*, *284*(4), F671–F679.

Lee, J. H., Kim, J. H., Kim, J. S., Chang, J. W., Kim, S. B., Park, J. S., & Lee, S. K. (2013). AMP-activated protein kinase inhibits TGF-beta-, angiotensin II-, aldosterone-, high glucose-, and albumin-induced epithelial-mesenchymal transition. *American Journal of Physiology. Renal Physiology*, *304*(6), F686–F697.

Ling, L., Chen, L., Zhang, C., Gui, S., Zhao, H., & Li, Z. (2018). High glucose induces podocyte epithelial to mesenchymal transition by demethylation mediated enhancement of MMP9 expression. *Molecular Medicine Reports*, *17*(4), 5642–5651.

Ling, L., Tan, Z., Zhang, C., Gui, S., Hu, Y., & Chen, L. (2018). Long noncoding RNA ENSRNOG00000037522 is involved in the podocyte epithelial mesenchymal transition in diabetic rats. *International Journal of Molecular Medicine*, *41*(5), 2704–2714.

Little, M. H., & McMahon, A. P. (2012). Mammalian kidney development: Principles, progress, and projections. *Cold Spring Harbor Perspectives in Biology*, *4*(5), a008300.

Liu, Y. (2010). New insights into epithelial-mesenchymal transition in kidney fibrosis. *Journal of the American Society of Nephrology*, *21*(2), 212–222.

Masson, E., Koren, S., Razik, F., Goldberg, H., Kwan, E. P., Sheu, L., … Fantus, I. G. (2009). High beta-cell mass prevents streptozotocin-induced diabetes in thioredoxin-interacting protein-deficient mice. *American Journal of Physiology, Endocrinology and Metabolism*, *296*(6), E1251–E1261.

Mathis, D., Vence, L., & Benoist, C. (2001). beta-Cell death during progression to diabetes. *Nature*, *414*(6865), 792–798.

Molitch, M. E., DeFronzo, R. A., Franz, M. J., Keane, W. F., Mogensen, C. E., Parving, H. H., & Steffes , M. W. (2004). Nephropathy in diabetes. *Diabetes Care*, *27*(Suppl 1), S79–S83.

Mundel, P., Reiser, J., Borja, A. Z., Pavenstädt, H., Davidson, G. R., Kriz, W., & Zeller, R. (1997). Rearrangements of the cytoskeleton and cell contacts induce process formation during differentiation of conditionally immortalized mouse podocyte cell lines. *Experimental Cell Research*, *236*(1), 248–258.

Nishikawa, T., Edelstein, D., Du, X. L., Yamagishi, S., Matsumura, T., Kaneda, Y., … Brownlee, M. (2000). Normalizing mitochondrial superoxide production blocks three pathways of hyperglycaemic damage. *Nature*, *404*(6779), 787–790.

Nishiyama, A., Matsui, M., Iwata, S., Hirota, K., Masutani, H., Nakamura, H., … Yodoi, J. (1999). Identification of thioredoxin-binding protein-2/vitamin D (3) up-regulated protein 1 as a negative regulator of thioredoxin function and expression. *Journal of Biological Chemistry*, *274*(31), 21645–21650.

Pavenstädt, H., Kriz, W., & Kretzler, M. (2003). Cell biology of the glomerular podocyte. *Physiological Reviews*, *83*(1), 253–307.

Perrone, L., Devi, T. S., Hosoya, K., Terasaki, T., & Singh, L. P. (2009). Thioredoxin interacting protein (TXNIP) induces inflammation through chromatin modification in retinal capillary endothelial cells under diabetic conditions. *Journal of Cellular Physiology*, *221*(1), 262–272.

Qi, W., Chen, X., Gilbert, R. E., Zhang, Y., Waltham, M., Schache, M., … Pollock, C. A. (2007). High glucose-induced thioredoxin-interacting protein in renal proximal tubule cells is independent of transforming growth factor-beta1. *American Journal of Pathology*, *171*(3), 744–754.

Quaggin, S. E., & Kreidberg, J. A. (2008). Development of the renal glomerulus: Good neighbors and good fences. *Development*, *135*(4), 609–620.

Rask-Madsen, C., & King, G. L. (2013). Vascular complications of diabetes: Mechanisms of injury and protective factors. *Cell Metabolism*, *17*(1), 20–33.

Sabatini, D. M. (2006). mTOR and cancer: Insights into a complex relationship. *Nature Reviews Cancer*, *6*(9), 729–734.

Sarbassov, D. D., Guertin, D. A., Ali, S. M., & Sabatini, D. M. (2005). Phosphorylation and regulation of Akt/PKB by the rictor-mTOR complex. *Science*, *307*(5712), 1098–1101.

Shah, A., Xia, L., Goldberg, H., Lee, K. W., Quaggin, S. E., & Fantus, I. G. (2013). Thioredoxin-interacting protein mediates high glucose-induced reactive oxygen species generation by mitochondria and the NADPH oxidase, Nox4, in mesangial cells. *Journal of Biological Chemistry*, *288*(10), 6835–6848.

Shah, A., Xia, L., Masson, E. A. Y., Gui, C., Momen, A., Shikatani, E. A., … Fantus, I. G. (2015). Thioredoxin-interacting protein deficiency protects against diabetic nephropathy. *Journal of the American Society of Nephrology*, *26*(12), 2963–2977.

Shi, Y., Ren, Y., Zhao, L., Du, C., Wang, Y., Zhang, Y., … Duan, H. (2011). Knockdown of thioredoxin interacting protein attenuates high glucose-induced apoptosis and activation of ASK1 in mouse mesangial cells. *FEBS Letters*, *585*(12), 1789–1795.

Sifuentes-Franco, S., Padilla-Tejeda, D. E., Carrillo-Ibarra, S., & Miranda-Díaz, A. G. (2018). Oxidative Stress, apoptosis, and mitochondrial function in diabetic nephropathy. *International Journal of Endocrinology*, *2018*, 1875870.

Strutz, F., & Zeisberg, M. (2006). Renal fibroblasts and myofibroblasts in chronic kidney disease. *Journal of the American Society of Nephrology*, *17*(11), 2992–2998.

Susztak, K., Raff, A. C., Schiffer, M., & Bottinger, E. P. (2006). Glucose-induced reactive oxygen species cause apoptosis of podocytes and podocyte depletion at the onset of diabetic nephropathy. *Diabetes*, *55*(1), 225–233.

Tan, S. M., Zhang, Y., Cox, A. J., Kelly, D. J., & Qi, W. (2011). Tranilast attenuates the up-regulation of thioredoxin-interacting protein and oxidative stress in an experimental model of diabetic nephropathy. *Nephrology, Dialysis, Transplantation*, *26*(1), 100–110.

Tanaka, Y., Kume, S., Kitada, M., Kanasaki, K., Uzu, T., Maegawa, H., & Koya, D. (2012). Autophagy as a therapeutic target in diabetic nephropathy. *Experimental Diabetes Research*, *2012*, 628978.

Um, S. H., D'Alessio, D., & Thomas, G. (2006). Nutrient overload, insulin resistance, and ribosomal protein S6 kinase 1, S6K1. *Cell Metabolism*, *3*(6), 393–402.

Wei, J., Shi, Y., Hou, Y., Ren, Y., Du, C., Zhang, L., … Duan, H. (2013). Knockdown of thioredoxin-interacting protein ameliorates high glucose-induced epithelial to mesenchymal transition in renal tubular epithelial cells. *Cellular Signalling*, *25*(12), 2788–2796.

Wu, J., Lin, H., Liu, D., Liu, J., Wang, N., Mei, X., … Zhang, X. (2013). The protective effect of telmisartan in Type 2 diabetes rat kidneys is related to the downregulation of thioredoxin-interacting protein. *Journal of Endocrinological Investigation*, *36*(7), 453–459.

Wu, M., Li, R., Hou, Y., Song, S., Han, W., Chen, N., … Shi, Y. (2018). Thioredoxin-interacting protein deficiency ameliorates kidney inflammation and fibrosis in mice with unilateral ureteral obstruction. *Laboratory Investigation*, *98*, 1211–1224.

Wullschleger, S., Loewith, R., & Hall, M. N. (2006). TOR signaling in growth and metabolism. *Cell*, *124*(3), 471–484.

Xu, Y., Liu, L., Xin, W., Zhao, X., Chen, L., Zhen, J., & Wan, Q. (2015). The renoprotective role of autophagy activation in proximal tubular epithelial cells in diabetic nephropathy. *Journal of Diabetes and its Complications*, *29*(8), 976–983.

Yang, J., & Liu, Y. (2001). Dissection of key events in tubular epithelial to myofibroblast transition and its implications in renal interstitial fibrosis. *American Journal of Pathology*, *159*(4), 1465–1475.

Zhang, H., Liu, C., Ma, Y., Xiao, L., Li, F., Ying, H., & Liu, H. (2015). Efficient preparation of a TXNIP knockout mouse model by transcription activator-like effector nucleases (TALEN). *Chinese Journal of Comparative Medicine*, *25*, 9–13.

How to cite this article: Song S, Qiu D, Shi Y, et al. Thioredoxin-interacting protein deficiency alleviates phenotypic alterations of podocytes via inhibition of mTOR activation in diabetic nephropathy. *J Cell Physiol*. 2019;1–18. https://doi.org/10.1002/jcp.28317